Available online at www.sciencedirect.com

ScienceDirect

Palaeoworld 30 (2021) 708–723

Palaeoworld

www.elsevier.com/locate/palwor

Revision of *Chunerpeton tianyiense* (Lissamphibia, Caudata): Is it a cryptobranchid salamander?

Yu-Fen Rong [a,b,c,d,e,*], Davit Vasilyan [d,e], Li-Ping Dong [a,c], Yuan Wang [a,c]

[a] *Key Laboratory of Vertebrate Evolution and Human Origins, Institute of Vertebrate Paleontology and Paleoanthropology, Chinese Academy of Sciences, Beijing, China*

[b] *University of Chinese Academy of Sciences, Beijing, China*

[c] *CAS Center for Excellence in Life and Paleoenvironment, Beijing, China*

[d] *JURASSICA Museum, Porrentruy, Switzerland*

[e] *Université de Fribourg, Fribourg, Switzerland*

Received 5 November 2020; received in revised form 15 November 2020; accepted 1 December 2020
Available online 8 December 2020

Abstract

Lacustrine deposits of Juro-Cretaceous age in northeastern China have yielded some of the best-preserved fossils of early crown salamanders. One of those taxa, *Chunerpeton tianyiense*, has been considered as a crown or stem member of the family Cryptobranchidae, significant for implying a long evolutionary history for cryptobranchids and for calibrating the molecular clock of Caudata evolution. Building on the most recent large-scale phylogenetic analysis of relationships among fossil and recent salamanders and utilizing new specimens of *Chunerpeton*, we update the osteological description and diagnosis for *Chunerpeton* and reconsider its phylogenetic relationships. On the basis of recently collected *Chunerpeton* skeletons from the type locality at Daohugou, Inner Mongolia, China and available literature, we update the taxon-character matrix and run phylogenetic analyses with constraints on the relationships among families using a molecular backbone. We redescribe the osteology of *Chunerpeton*, revise and identify some new characters including large anterodorsal fenestra bordered by paired premaxillae, nasals, and frontals; nasals separate and wider than frontal; contact between nasal and prefrontal present; lacrimal present; and contact between pterygoid and parasphenoid absent. Osteological comparisons between *Chunerpeton* and living cryptobranchids reveal a suite of distinct differences in snout shape and in configurations, positions, and contacts of certain skull bones. Our phylogenetic analyses consistently place *Chunerpeton* as a stem Caudata outside of Cryptobranchidae and crown salamanders. Exclusion of *Chunerpeton* from Cryptobranchidae will require reconsideration of the origin time for Cryptobranchidae and recalibration of the molecular clock for the whole caudatan tree.

Keywords: *Chunerpeton*; Cryptobranchidae; China; Late Jurassic; Osteology; Phylogeny

1. Introduction

The family Cryptobranchidae includes the world's largest known extant caudates, namely the Chinese and Japanese giant salamanders. Cryptobranchids are represented by two living aquatic genera: *Andrias* and *Cryptobranchus*. *Andrias* contains the exclusively Japanese species *A. japonicus*, as the sister to a clade containing the exclusively Chinese species *A. davidianus*, *A. sligoi*, and an undescribed species, whereas the monospecific *Cryptobranchus*, with the species *C. alleganiensis*, lives in the eastern USA (e.g., Duellman and Trueb, 1994; Turvey et al., 2019). Cryptobranchidae are nested together with their sister family Hynobiidae within the clade of Cryptobranchoidea (e.g., Wiens et al., 2005; Pyron and Wiens, 2011).

* Corresponding author.
E-mail address: rongyufen@ivpp.ac.cn (Y.F. Rong).

https://doi.org/10.1016/j.palwor.2020.12.001

Over the past quarter-century, thousands of well-preserved salamander skeletons have been discovered in Jurassic–Cretaceous strata in northeastern China. About a dozen species have been formally named and some have been assigned to living clades. These taxa are important for documenting the early evolutionary diversification and radiation of salamanders (e.g., Gao and Shubin, 2003; Gao et al., 2013; Jia and Gao, 2016a, 2019). One of the geologically oldest species, *Chunerpeton tianyiense*, was described as belonging to the extant family Cryptobranchidae (Gao and Shubin, 2003).

Subsequent phylogenetic analyses typically grouped *Chunerpeton* with the cryptobranchids and placed it as either a crown or stem member (Gao and Shubin, 2003; Wang and Evans, 2006; Jia and Gao, 2016a, 2019; Rong, 2018), but the cryptobranchid affinities of *Chunerpeton* were questioned by Vasilyan et al. (2013). As the presumed earliest cryptobranchid, *Chunerpeton* has been used to calibrate the molecular clock for the split between Cryptobranchidae and Hynobiidae (e.g., San Mauro et al., 2005; Bossuyt et al., 2006; Chen et al., 2015; Irisarri et al., 2017). Its position near the base of the salamander tree also makes *Chunerpeton* useful for dating the origin of Caudata (the total group) and the split between Cryptobranchoidea and Salamandroidea.

In the short type description for *Chunerpeton tianyiense* by Gao and Shubin (2003), just four catalogued specimens were listed, only the holotype was figured, and a limited number of osteological characters were listed in the diagnosis. The authors questionably identified a hypohyal (Gao and Shubin, 2003, pp. 425–426, text-figs. 1b, 2b), an element that is not ossified in the hyobranchium of living cryptobranchids. Several subsequent studies on *Chunerpeton* provided revised diagnoses of *Chunerpeton*, suggested that *Chunerpeton* and *Beiyanerpeton* might be synonyms (Sullivan et al., 2014), and reported their prey preferences for the corixid *Yanliaocorixa chinensis* (Dong et al., 2011) and limb abnormalities (Wang et al., 2015). Despite the above-cited work and the fact that *Chunerpeton* is known by hundreds of skeletons from at least six localities (e.g., Sullivan et al., 2014), a detailed understanding of its osteology is still pending. That situation is unfortunate, given that *Chunerpeton* is a key genus for deciphering the early evolutionary history of salamanders. Here we address those deficiencies by using additional skeletons of *C. tianyiense* from the type locality to present an updated diagnosis and a more detailed osteological description for the species and to reevaluate its phylogenetic affinities.

Institutional abbreviations

CAGS: Chinese Academy of Geological Sciences, Beijing, China.
IVPP: Institute of Vertebrate Paleontology and Paleoanthropology, Chinese Academy of Sciences, Beijing, China.
ZFMK: Zoologisches Forschungsmuseum Koenig, Bonn, Germany.

2. Materials and methods

Our study relies on 31 referred fossil skeletons of *Chunerpeton tianyiense*, all collected from the type locality (i.e., Daohugou locality, Ningcheng County, Inner Mongolia, China) and deposited in the collections of IVPP. We examined specimens using a Leica binocular microscope and photographed using NIKON D850 and NIKON D7000 digital cameras. We created the photographic illustrations using Photoshop CS6 and the line drawings using Illustrator CS5. Our anatomical nomenclature generally follows Francis (1934), but for specific bones or regions follows Rose (2003) and Vasilyan et al. (2013).

According to Article 34.2 of the 4th Edition of the International Code of Zoological Nomenclature (International Commission on Zoological Nomenclature, 1999), "The ending of a Latin or latinized adjectival or participial species-group name must agree in gender with the generic name with which it is at any time combined [Art. 31.2]; if the gender ending is incorrect it must be changed accordingly (the author and date of the name remain unchanged [Art. 50.3.2])." The Greek word "herpeton" is neuter, meaning the corresponding specific names should also be neuter. Therefore, the following names are corrected for the six species of Chinese Mesozoic salamanders: *Sinerpeton fengshanense* Gao and Shubin, 2001, Chunerpeton tianyiense Gao and Shubin, 2003, Pangerpeton sinense Wang and Evans, 2006, Regalerpeton weichangense Zhang et al., 2009, Beiyanerpeton jianpingense Gao and Shubin, 2012, and Nuominerpeton aquilonare Jia and Gao, 2016b, and all with neuter -e instead of masculine and feminine -is.

3. Systematic paleontology

Class Amphibia Linnaeus, 1758
Subclass Lissamphibia Haeckel, 1866
Order Caudata Scopoli, 1777

Genus *Chunerpet*on Gao and Shubin, 2003
Type species: Chunerpeton tianyiense Gao and Shubin, 2003.
Diagnosis: Same as for the type and only species.

Chunerpeton tianyiense Gao and Shubin, 2003
(Figs. 1–3, 4A–C)

Holotype: CAGS-IG-02051, natural molds of dorsal and ventral aspects of an articulated, subadult skeleton preserving skull and postcranium (Gao and Shubin, 2003, pp. 425–426, text-figs. 1, 2).
Emended diagnosis (updated from Gao and Shubin, 2003): Ribs unicapitate (Gao and Shubin, 2003); three paired ribs bearing anterior caudal vertebrae (Gao and Shubin, 2003); internal carotid foramina penetrate parasphenoid (Gao

Fig. 1. Photographs of a nearly complete skeleton of *Chunerpeton tianyiense* (IVPP V 13343A&B) from the Jurassic of China. (A) Dorsal view of skeleton on slab IVPP V 13343A. (B) Ventral view of skeleton on slab IVPP V 13343B. Abbreviations: fe, femur; fi, fibula; hu, humerus; il; ilium; isc, ischium; ra, radius; sca, scapulocoracoid; sv, sacral vertebra; ti, tibia; ul, ulna. Photograph source credit: Wei Gao.

and Shubin, 2003); well-developed anterolateral process of parietal extending along lateral border of frontal (Gao and Shubin, 2003); frontal-maxilla contact absent (Gao and Shubin, 2003); parietal-prefrontal contact absent (Gao and Shubin, 2003); anteromedial fenestra present (Gao and Shubin, 2003); pars praenasalis of premaxilla midline contact absent (Gao and Shubin, 2003); vomers without posterior extension (Gao and Shubin, 2003); paired hypobranchial I and II ossified (Gao and Shubin, 2003); basibranchial II arrow-shaped (Gao and Shubin, 2003); 16 presacral vertebrae (Gao and Shubin, 2003); nasals without midline contact (contra lacking midline contact of dorsal processes of premaxillae according to Gao and Shubin, 2003); nasal-prefrontal contact present (contra nasal-prefrontal contact absent according to Gao and Shubin, 2003); nasal wider than frontals (contra nasals narrower than frontals according to Gao and Shubin, 2003); lacrimal present and contributing to external naris, but not to orbit (contra lacrimal absent according to Gao and Shubin, 2003); anterodorsal fenestra formed by premaxilla, nasal and frontal (contra anterodorsal fenestra formed only by premaxilla and nasal according to Jia and Gao, 2019); single vomerine tooth row parallel to premaxillary and maxillary tooth rows (new); pterygoid triradiate with a slender dentate anteromedial process (new); palatine present (new); prootic, exoccipital and opisthotic present as separate bones (new).

Type locality and horizon: Daohugou, Ningcheng County, Inner Mongolia, China; Haifanggou Formation; Late Jurassic, 163 Ma (Liu et al., 2006; Huang, 2015).

Referred material: Part and counterpart slabs are identified with the suffixes "A&B", and single slab is identified without suffix. IVPP V 11976, ventral impression of articulated skeleton lacking most of skull; V 12609, an incomplete dorsal skeleton impression lacking most of skull; V 12611, an incomplete ventral skeleton impression lacking anterior part of skull and posterior part of tail; V 13241A&B, articulated skeleton impression; V 13343A&B, nearly complete skeleton impression with part of tail missing; V 13478, articulated natural molds of bones without skull preserved in lateral view; V 14051A&B, articulated skeleton impression lacking pelvic girdle and tail; V 14052, nearly complete dorsal skeleton impression; V 14054A&B, nearly complete skeleton impression; V 14055A&B, nearly complete skeleton impression with part of tail missing; V 14056, incomplete ventral skeleton impression lacking part of tail; V 14058A&B, articulated natural molds of skeleton with part of tail missing; V 14060A&B, nearly completely articulated natural molds of skeleton; V 14063, incomplete natural molds of skull preserved in dorsal view; V 14220A&B, articulated skeleton impression; V 14221A&B, articulated skeleton impression; V 14222A&B, incomplete skeleton impression lacking pelvic girdle and tail; V 14223A&B, incomplete skeleton impression with six presacral vertebrae, pelvic girdle and fifteen caudal vertebrae; V 14224A&B, incomplete skeleton impression lacking part of skull and pelvic girdle and tail; V 14225, incomplete ventral skeleton impression; V 14226A&B, incomplete skeleton impression with the tail missing; V 14227A&B, nearly complete skeleton impression; V 14228A&B, incomplete skull impression; V 14250A&B, incomplete skeleton with part of skull and tail missing; V 14254, incomplete ventral skeleton impression with skull and nine presacral vertebrae; V 14256A&B, incomplete skull and part appendicular skeleton; V 14429A&B, nearly complete natural molds of skeleton with axial skeleton preserved in impression; V 14604A&B, nearly complete skeleton impression; V 14609, ventral skull impression; V 14745, nearly complete dorsal skeleton impression lacking part of the tail; V 15422, incomplete natural molds of skeleton in ventral view.

4. Description

4.1. General features

All studied specimens are preserved in articulation as natural impressions or some with bones on part and counterpart slabs or a single slab. They represent individuals of different size and the snout-pelvic length ranges from 20 mm (IVPP V 13241A&B) to 115 mm (IVPP V 15422). *Chunerpeton* is a neotenic salamander, with a short, broad, and rounded snout. The skull is slightly longer than wide. The preserved soft tissue impressions indicate that *Chuner-*

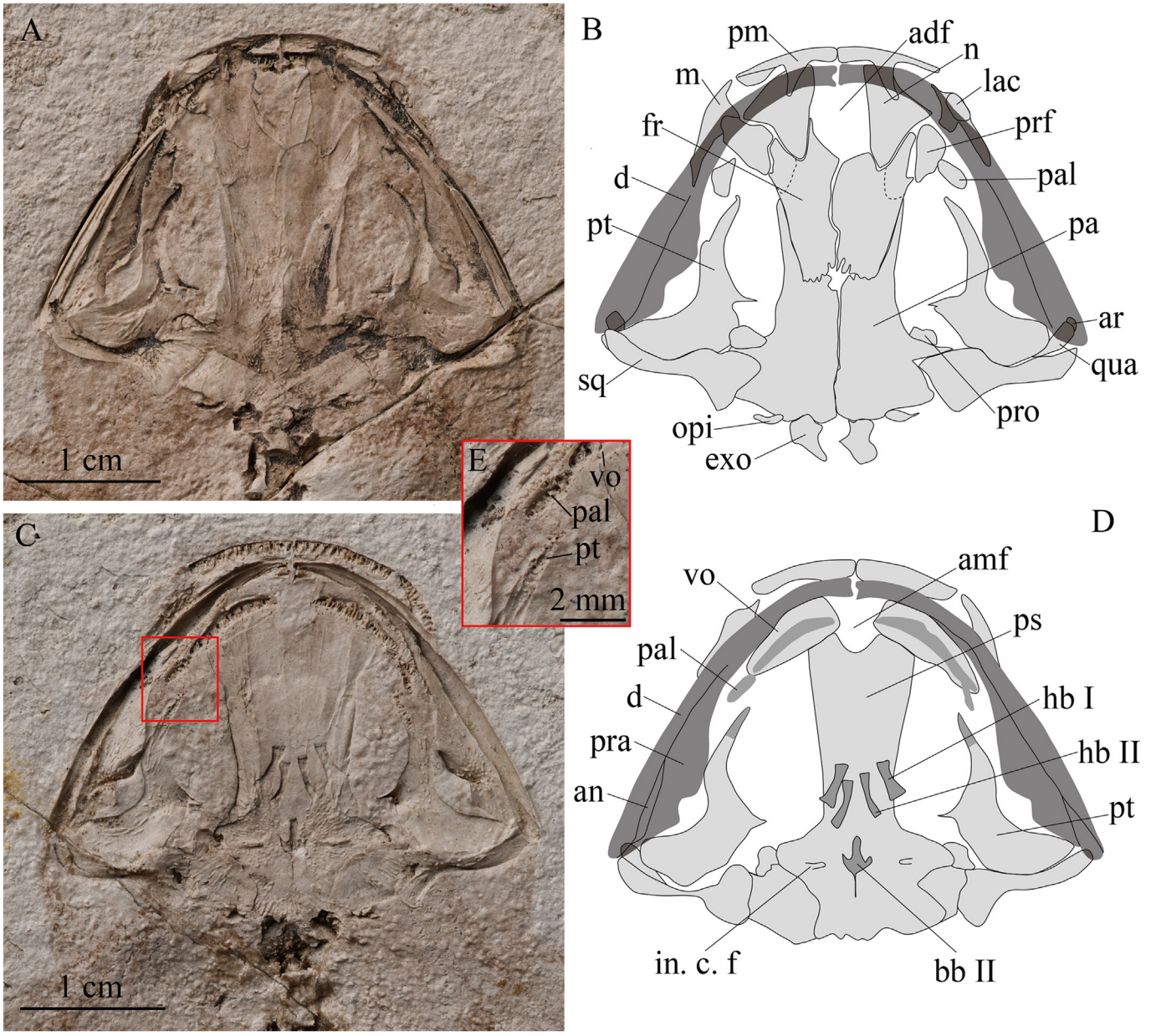

Fig. 2. Close-up of the skull of *Chunerpeton tianyiense* (IVPP V 13343A&B) from the Jurassic of China (see Fig. 1 for entire specimen). (A, B) Dorsal impressions of skull on slab IVPP V 13343A, photograph (A) and interpretive line drawing (B). (C, D) Ventral impressions of skull on slab IVPP V 13343B, photograph (C) and interpretive line drawing (D). (E) Close-up of palatal region, denoted by red box in (C) showing right palatine and portions of adjacent pterygoid and vomer, in ventral view. For interpretive drawings: dark grey shading denotes mandibles, medium grey shading denotes palatal tooth rows, light grey shading denotes skull bones, and dashed lines on frontals indicate correct anatomical positions for the displaced prefrontals. Abbreviations: adf, anterodorsal fenestra; amf, anteromedial fenestra; an, angular; ar, articular; bb II, basibranchial II; d, dentary; exo, exoccipital; fr, frontal; hb I–II, hypobranchial I–II; in. c. f, internal carotid foramen; lac, lacrimal; m, maxilla; n, nasal; opi, opisthotic; pa, parietal; pal, palatine; pm, premaxilla; pra, prearticular; prf, prefrontal; pro, prootic; ps, parasphenoid; pt, pterygoid; qua, quadrate; sq, squamosal; vo, vomer. Photograph source credit: Wei Gao.

peton had three pairs of densely-branched external gills bearing branchial teeth (Figs. 1, 2A, C, 3A–C). The skull roof has a distinct and large anterodorsal fenestra bordered by the paired premaxillae, nasals, and frontals (Figs. 2A, B, 4A), an observation differing from that of Gao and Shubin (2003, p. 426, text-fig. 2b) which excluded the frontal. A recent study has recognized five patterns of anterodorsal fenestrae for living salamanders that shows this feature has taxonomic significance (Jia and Gao, 2019). Thus, the framing of the anterodorsal fenestra of *Chunerpeton* by the paired premaxillae, nasals, and frontals is identified as a diagnostic character. The palate consists of paired vomers, palatines, and pterygoids, and a broad parasphenoid. The vomerine teeth are monostichous and arranged in a single, curved line extending parallel to the premaxillary and maxillary tooth rows. The fore- and hindlimbs

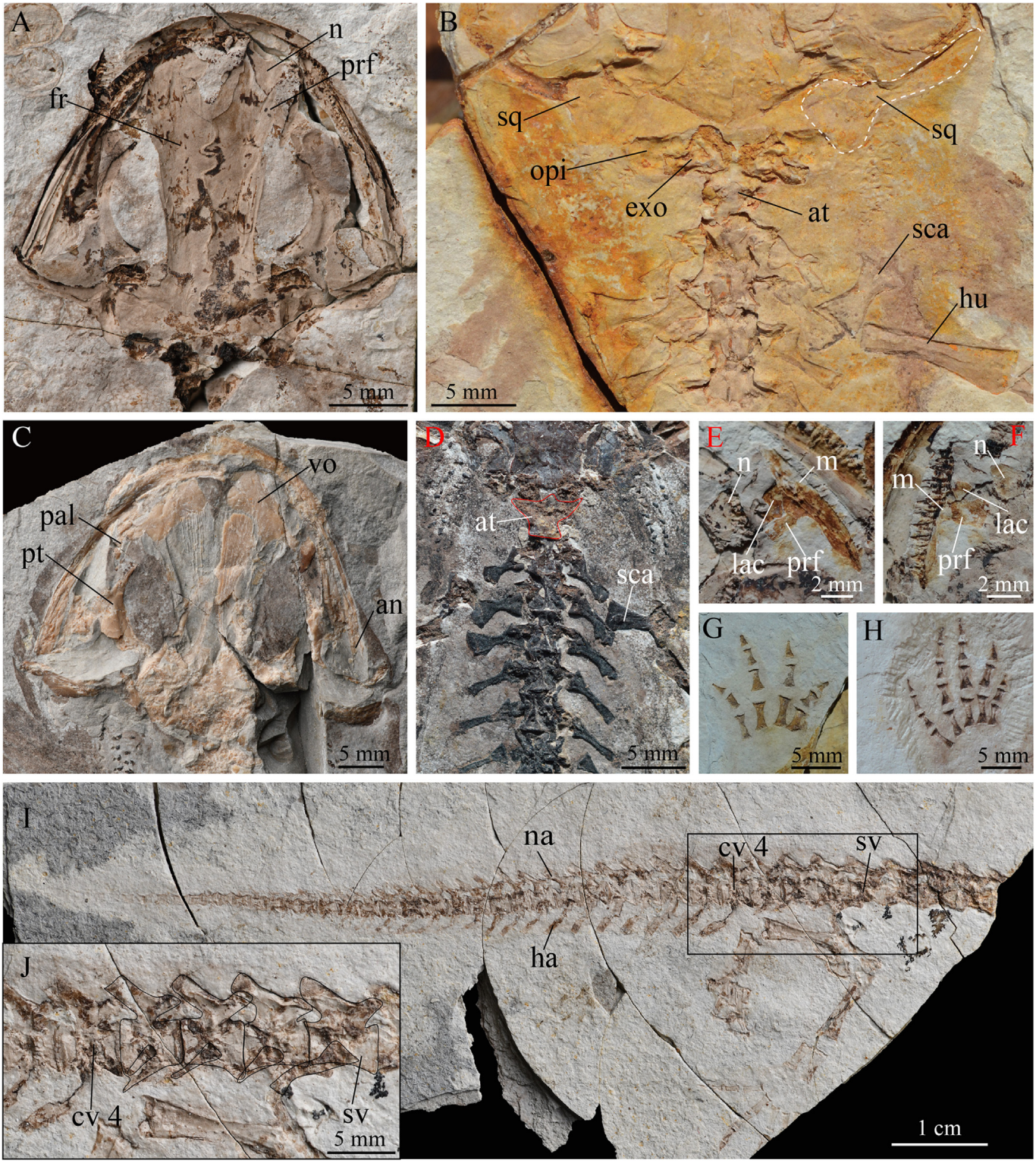

Fig. 3. Photographs of referred skeletons of *Chunerpeton tianyiense* from the Jurassic of China. (A) Dorsal impression of skull on slab IVPP V 14226A. (B) Dorsal impression of the otico-occipital region and anterior trunk on slab IVPP V 14745. (C) Ventral views of skull on slab IVPP V 15422. (D) Ventral view of anterior part of vertebrae on slab IVPP V 14058A. (E, F) Dorsal (E) and ventral (F) impressions of articulated maxilla, lacrimal, and prefrontal on slabs IVPP V 14228A and IVPP V 14228B, respectively. (G, H) Impressions of left manus (G) and left pes (H) on slabs IVPP V 11976 and IVPP V 14055, respectively. (I) Lateral view of the tail, also includes posterior trunk vertebrae and sacrum, pelvic girdle, and hindlimbs on slab IVPP V 14054. (J) Close-up of the anterior caudal region, denoted by black box in (I), showing the first three caudal vertebrae bearing ribs, in lateral view. Abbreviations: an, angular; at, atlas; cv 4, the fourth caudal vertebra; exo, exoccipital; fr, frontal; ha, haemal arch; hu, humerus; lac, lacrimal; m, maxilla; n, nasal; na, neural arch; opi, opisthotic; pal, palatine; prf, prefrontal; pt, pterygoid; sca, scapulocoracoid; sq, squamosal; sv, sacral vertebra; vo, vomer. Photograph source credit: Wei Gao.

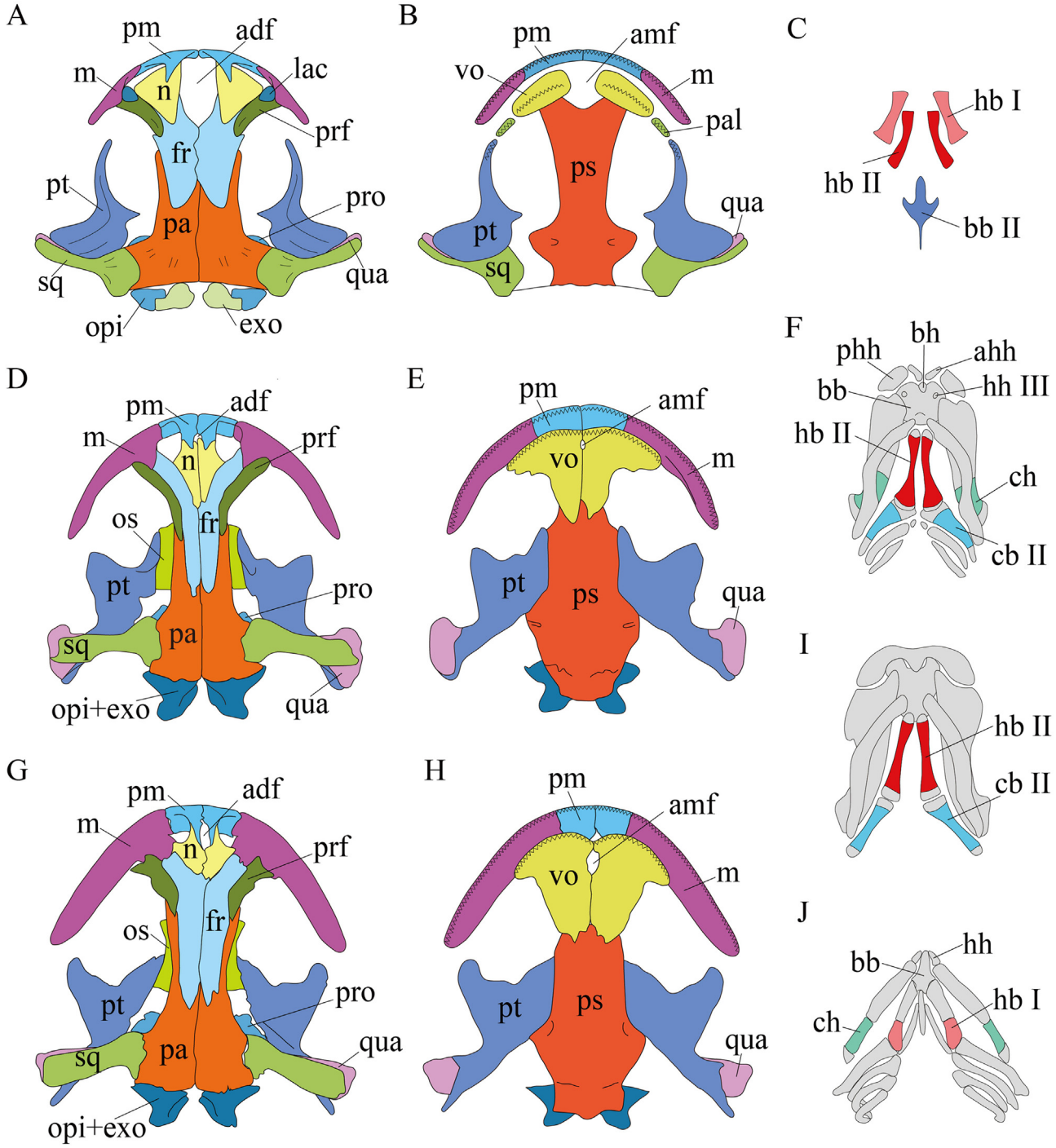

Fig. 4. Color-coded line drawings of skulls and hyobranchium of *Chunerpeton tianyiense* and representative living cryptobranchids, plus hyobranchium of paedomorphic *Ichthyosaura alpestris*. Images not to scale. (A–C) Reconstruction of *Ch. tianyiense*, dorsal (A) and ventral (B) views of skull and ventral view (C) of hyobranchium. (D–F) *Cryptobranchus alleganiensis*, dorsal (D) and ventral (E) views of skull and ventral view (F) of hyobranchium. (G–I) *Andrias davidianus* (ZFMK 90469), dorsal (G) and ventral (H) views of skull and ventral view (I) of hyobranchium. (J) *Ichthyosaura alpestris*, ventral view of hyobranchium. Grey shading denotes unossified hyobranchial elements. (D) and (E) are redrawn from Carroll and Holmes (1980), (F) and (I) from Rose (2003), and (J) from Heiss and Grell (2019). Abbreviations: adf, anterodorsal fenestra; ahh, anterior hypohyal; amf, anteromedial fenestra; an, angular; ar, articular; bb, basibranchial; bh, basihyal; bb II, basibranchial II; cb II, ceratobranchial II; ch, ceratohyal; exo, exoccipital; fr, frontal; hb I–II, hypobranchial I–II; hh, hypohyal; hh III, third hypohyal; lac, lacrimal; m, maxilla; n, nasal; opi, opisthotic; opi + exo, fused opisthotic + exoccipital; pa, parietal; pal, palatine; phh, posterior hypohyal; pm, premaxilla; prf, prefrontal; pro, prootic; ps, parasphenoid; pt, pterygoid; qua, quadrate; sq, squamosal; vo, vomer.

are well developed. The tail is laterally compressed, with tall neural and deep haemal arches; for a given caudal vertebra, its haemal arch is slightly longer than its neural arch (Fig. 3I).

4.2. Skull

The paired premaxillae (Figs. 2A, B, 4A) are thin, with moderately-long medial portions where the bones articulate across the skull midline. The premaxilla dorsally bears a small, triangular pars praenasalis that posteriorly overlaps the nasal (Figs. 2A, B, 4A), which contrasts with the original publication where the pars praenasalis was described as large and broad (Gao and Shubin, 2003, p. 426, text-fig. 2b). The lateral portion of the premaxilla for *Chunerpeton* is slightly longer and more slender than its medial portion, and its lateral end articulates with the anterior process of the maxilla. The premaxillary pars dentalis bears about 23 closely arranged pedicellate and monocuspid teeth. The pars palatina is reduced or absent (Figs. 2C, D, 4B).

A complete maxilla preserved as part of IVPP V 14228A&B (Fig. 3E, F) bears a moderately-developed anterior process. About 20 teeth are observable on the pars dentalis. The maxillary posterior process is longer than its anterior one. The maxilla bears a small and triangular facial process that contacts dorsally with the nasal and lacrimal (Figs. 3E, F, 4A). The maxillary pars palatina is reduced (Fig. 3F).

The paired nasals (Figs. 2A, B, 4A) are large, broad, and triangular in contrast to the original publication where the nasals were described as small, narrow, and elongated (Gao and Shubin, 2003, p. 426, text-fig. 2b). The pars praenasalis of the premaxilla covers the anterior process of the nasal. The posterolateral edge of the nasal contacts the prefrontal whereas the original publication states that a nasal-prefrontal contact is absent (Gao and Shubin, 2003, p. 426, text-fig. 2b). The nasal is wider than the frontal in contrast to the original description where the nasal was said to be narrower than the frontal (Gao and Shubin, 2003, p. 426, text-fig. 2b). The posterior process of the nasal overlies the frontal. The nasals are broadly separated across the skull midline by a large anterodorsal fenestra (Fig. 4A) in contrast with the original publication where a midline contact of nasals was described as present (Gao and Shubin, 2003, p. 426, text-fig. 2b).

The prefrontal (Figs. 2A, B, 4A) is triangular. Its medial part overlies the frontal, whereas its anteromedial edge contacts the nasal and lacrimal (Fig. 4A). The prefrontal does not articulate with the parietal.

The lacrimal (Fig. 3E, F, 4A) is a small bone that contacts the nasal and prefrontal, and contributes to the external narial margin, whereas the original description described the lacrimal as absent (Gao and Shubin, 2003). We did not observe a septomaxilla in any of our specimens.

The paired frontals (Figs. 2A, B, 4A) are roughly rectangular in shape. The anterior portion of the frontal is covered by the nasal and prefrontal in contrast to the original description where the frontals were said to extend anteriorly to the lateral border of the nasal (Gao and Shubin, 2003). The anterior portion of the frontal is developed into two large, lobe-like anterior processes and, more laterally, a smaller and pointed process. The suture between the frontals is wavy (Fig. 2A, B). The posterior end of the frontal articulates with the anterior portion of the parietal. A distinct median opening surrounded by both frontals and parietals is observable in IVPP V 13343A (Fig. 2A, B). However, that opening is not present in IVPP V 14226A (Fig. 3A) or in the holotype (Gao and Shubin, 2003, p. 426, text-fig. 2).

The parietals (Figs. 2A, B, 4A) are large bones located behind the frontals. The parietal has a wide lateral extension that articulates with the proximal head of the squamosal (Fig. 3B). The parietal bears a long anterolateral process extending along the lateral edge of the frontal, but that process does not extend far enough anteriorly to articulate with the prefrontal (Figs. 2A, B, 3A, 4A). In IVPP V 13343A, the dorsal surface of the parietal is weakly sculpted with irregular, curved low ridges (Fig. 2A), but in IVPP V 14226A the same surface is smooth (Fig. 3A).

The paired squamosals (Figs. 2A, B, 3B, 4A) are elongate bones that form the posterolateral margin of the skull. The squamosal is positioned transversely and inclines slightly anteriorly. The proximal head of the squamosal is triangular and articulates medially with the parietal. The quadrate ramus is gracile and articulates ventrally with the quadrate. Preserved impressions of the squamosal show that the external surface of the caput squamosi is weakly sculptured in IVPP V 13343A, but the same surface in IVPP V 14745 is smooth (cf. Fig. 2A versus Fig. 3B).

The paired quadrates (Fig. 2A–D) are triangular bones sandwiched between the squamosal and the lateral process of the pterygoid.

The pterygoid (Figs. 2, 3A, C, 4A, B) is triradiate, consisting of a central portion and the anteromedial, medial, and lateral processes. The anteromedial process is long, slender and curved. Its anterior tip is medially orientated and free of bony contacts. About ten teeth are observable in a single row on the anterior end of the anteromedial process (e.g., IVPP V 13343: Fig. 2C–E). The pterygoid teeth are present even in the largest individuals (skull length = 3 cm) that we examined (e.g., IVPP V 15422: Fig. 3C). The medial process of the pterygoid is small and free of bony contacts (Figs. 2, 3A, 4A). The lateral process of the pterygoid is large, wide and articulates dorsally with both the quadrate and squamosal (Fig. 4A, B). In most adult salamanders, the pterygoid (if present) is toothless (but dentate in *Necturus*) and has various shapes (e.g., Duellman and Trueb, 1994; Rose, 2003). The triradiate pterygoid with a slender dentate anteromedial process is a newly identified feature for *Chunerpeton*.

The paired vomers (Figs. 2C, D, 4B) are located at the anterior portion of the palate. They do not meet the premaxillae and maxillae, but articulate posteriorly with the anterior process of the parasphenoid. The vomers are broadly separated from each other across the skull midline by the anteromedial fenestra. They are long, narrow, and slightly curved. Approximately 28 teeth are present and aligned in a row paralleling the posterior portion of the premaxillary tooth row and the anterior portion of the maxillary tooth row (Fig. 2C). Rare, preserved tooth crowns indicate that the vomerine teeth are pedicellate and monocuspid. In living salamanders, the arrangement and position of the vomerine teeth has ontogenetic and taxonomic significance (e.g., Rose, 2003). Given that the vomerine teeth retain the same shape and position in different size *Chunerpeton*, a single vomerine tooth row parallel to the premaxillary and maxillary tooth row is identified as a new diagnostic character for *Chunerpeton*.

The paired palatines (Fig. 2E) are small bones located behind the vomer. The palatine does not contact any adjacent bones. The palatine tooth row consists of ten teeth. The teeth are similar in structure to those on the vomer and are arranged in a single row paralleling the posterior portion of the maxillary tooth row. Palatine teeth are present in all studied individuals, independent of body size; e.g., IVPP V 13343B (Fig. 2E) and IVPP V 15422 (Fig. 3C). The paired, dentate palatines are a newly identified feature which was not mentioned in the original description (Gao and Shubin, 2003, although it is illustrated, but not labeled, in text-fig. 2b).

The parasphenoid (Figs. 2C, D, 4B) is a large bone located along the ventral midline of the skull. It occupies about four-fifths of the total skull length. Two anterior processes are present and separated by a deep, U-shaped notch. Each of the anterior processes articulates with its corresponding vomer. Paired internal carotid foramina (Fig. 2C, D) are present in the lateral extensions of the parasphenoid.

The prootic, opisthotic, and exoccipital (Figs. 2B, 3B, 4A) are neither fused together, nor with other skull bones, even in large-sized individuals (e.g., IVPP V 14745: Fig. 3B). Details of those bones cannot be seen, due to crushing in that region of the skull. Different levels of fusion among prootic, opisthotic, and exoccipital occurs in living salamanders, such as three elements without fusion in proteids, fused exoccipital + opisthotic with separate prootic in most cryptobranchoids, fused prootic + opisthotic with separate exoccipital in sirenids, and all three elements fused in most salamandroids (e.g., Duellman and Trueb, 1994; Rose, 2003). Thus, the presence of a separate prootic, exoccipital, and opisthotic is treated as a new diagnostic character for *Chunerpeton*. The paired orbitosphenoids form the bony lateral wall of braincase in most mature salamanders except proteids (Rose, 2003). We did not observe an orbitosphenoid in any of our specimens.

4.3. Lower jaw

The lower jaw (Fig. 2C, D) consists of the dentary, prearticular, articular, and angular. The dentary and prearticular form, respectively, the majority of the labial and lingual surfaces of the lower jaw (Fig. 2C, D). The dentary bears a row of 50 teeth that are closely packed, narrow, pedicellate, and monocuspid. The angular (Figs. 2C, D, 3C) is a narrow bone sandwiched between the dentary and prearticular. The angular has a pointed anterior end (Fig. 3C) and it does not fuse with the prearticular. The articular is a tiny bone located at the posterior end of the lower jaw, where it articulates with the quadrate to form the skull-jaw joint (Fig. 2A, B).

4.4. Hyobranchium

The ossified hyobranchial elements consist of paired hypobranchial I and II and a single, median basibranchial II (Figs. 2C, D, 4C). The paired second hypobranchials are located posteromedially to the first hypobranchials, whereas basibranchial II is located directly behind them along the skull midline. Hypobranchial I and II are both rod-shaped and laterally curved. Basibranchial II is arrow-shaped with an elongated and needle-like posterior process.

4.5. Axial skeleton

Chunerpeton has 15 presacral (one atlas and 14 trunk vertebrae), one sacral, and at least 38 caudal vertebrae (Gao and Shubin, 2003, pp. 425–426, text-figs. 1a, 2a; Figs. 1, 3I). The atlas is the same length as the following trunk vertebrae (Fig. 3D). Anteriorly, the atlas bears a small and triangular tuberculum interglenoideum (sensu Evans and Milner, 1996) arising between a pair of broad anterior cotyles, the latter being firmly articulated with the occipital condyles on the skull. No free ribs or transverse processes are observable on the atlas (Fig. 3B, D). The trunk vertebrae are amphicoelous and, on either side, bear a relatively short and unicapitate transverse process that articulates distally with a rib (Fig. 3D). The first three pairs of ribs are more massive than the following ones, and have expanded proximal and distal ends (Fig. 3D), serving as attachment surfaces for the pectoral musculature (Francis, 1934). All trunk ribs are unicapitate and, from the fourth pair back, they gradually reduce in size. The last pair of trunk ribs is triangular (Fig. 1). The sacral ribs, for articulation with the pelvis, are larger than the most anterior trunk ribs (Fig. 3J). IVPP V 14054 (Fig. 3I, J) shows that the first three caudal vertebrae bear ribs. Starting with the fourth caudal vertebra, all remaining caudals lack free ribs, but they bear distinct neural and haemal arches (Fig. 3I). The haemal arch of a given caudal vertebra is longer than its neural arch (Fig. 3I).

4.6. Appendicular skeleton

The pectoral girdle consists of a pair of scapulocoracoids (Figs. 1A, 3D). In each, the coracoid portion is triangular and the scapular portion has an expanded distal end. The proximal end of the humerus is wider than the distal end (Fig. 1A) and its shaft bears a distinct crista ventralis. The radius and ulna are both straight, with the ulna slightly longer than the radius. The carpals are not ossified (Fig. 3G). The phalangeal formula is 2-2-3-2 in both IVPP V 13343 (Fig. 1A) and IVPP V 11976 (Fig. 3G).

The pelvic girdle consists of the paired ilia and ischia. The ilium is waisted and slightly curved (Fig. 1A). The ischium in IVPP V 14250 is large and blade-shaped. Both femora are detached from the pelvis in IVPP V 13343 (Fig. 1). The femur has a straight shaft and expanded proximal and distal ends (Figs. 1, 3I). The tibia and fibula are straight bones, both much shorter than the femur (Fig. 1). The tibia is shorter and more robust than the fibula. The tarsals are not ossified (Fig. 3H). In IVPP V 13343A, the phalangeal formula of the left pes is 2-2-2-2-2, and 2-3-3-3-2 for the right pes (Fig. 1). However, the right phalangeal formula is 2-2-3-4-3 in IVPP V 14055 (Fig. 3H).

4.7. Taxonomic identification

The 31 salamander skeletons we examined can be referred to *Chunerpeton tianyiense* based on the following combination of characters they share with the holotype (see Gao and Shubin, 2003): large anterodorsal fenestra formed by premaxillae, nasals, and frontals; pterygoid bearing a long, slender, curved, and free anteromedial process, and bearing a small, pointed, and free medial process, and bearing a large, wide lateral process; oval vomer, broadly separated across the skull midline, and with their long axis paralleling the premaxillae and maxillae, but not contacting those upper jaw bones; vomerine teeth in single row paralleling the premaxillary and the maxillary teeth; longer parasphenoid occupying posterior four-fifths of head length, and bearing two anterior processes separated by a deep, U-shaped notch; same configuration for hyobranchium consisting of paired hypobranchials I and II, and an arrow-shaped basibranchial II; 15 presacral vertebrae; and scapulocoracoid with triangular coracoid portion.

5. Comments on the skull and hyobranchium of *Chunerpeton*

Gao and Shubin's (2003) type description for *Chunerpeton tianyiense* was limited exclusively to characters they considered diagnostically informative. Our study expands on that original description, by providing a more detailed osteological description for the species. In particular, our study clarifies and reveals new aspects of cranial structure in *Chunerpeton*. We have been able to (1) reinterpret the relative size of the anterodorsal fenestra and show that it is bordered by the premaxillae, nasals, and frontals; (2) reinterpret the shapes and contacts of the premaxillae, nasals, and prefrontals; (3) reinterpret the elements identified as the vomer and nasal by Gao and Shubin (2003, p. 426, text-fig. 2b) as, respectively, the nasal and premaxilla; (4) establish that the pterygoid is triradiate with a slender dentate anteromedial process; (5) provide a detailed description of the palatal dentition; (6) confirm that free palatines are present; and (7) establish that the prootic, opisthotic and exoccipital are three separate bones. We are unable, however, to resolve the identity of a pair of prominent, subcircular structures, located to either side of the midline and about midway along the anteroposterior axis in the holotype skull, which were tentatively identified as hypohyals by Gao and Shubin (2003, pp. 425–426, text-figs. 1b, 2b). None of the *Chunerpeton* skeletons we examined preserves comparable structures, meaning that for the time being any discussion of those problematic structures relies on the holotype. In extant neotenic salamanders (e.g., *Amphiuma means*, *Necturus maculosus*, *Ichthyosaura alpestris*), the paired hypohyals lie near the anteromedial end of the hypobranchium and are relatively small and unossified elements (Fig. 4J), but in extant cryptobranchids the hypohyals are unossified and separated into anterior and posterior hypohyals (Fig. 4F), and a small, paired third hypohyal is possibly the result of resorption that detaches the anterior ceratohyal process from the rest of the larval ceratohyal cartilage (Rose, 2003; Heiss and Grell, 2019).

Although the shape and relative size of the problematic elements in the holotype of *Chunerpeton* are reminiscent of the posterior hypohyals in extant cryptobranchids (cf. Gao and Shubin, 2003, p. 425, text-fig. 1b versus Fig. 4F), we note that the shape, size, and position of those problematic elements suggest an alternative interpretation — that they may represent the orbitosphenoids forming the walls of the braincase. Clearly, examination of additional specimens will be required to resolve the identity of that element.

Below we compare *Chunerpeton* to other relevant salamanders and assess its phylogenetic relationships. Because many extinct salamander species are known by isolated and often fragmentary bones (e.g., Gardner and DeMar, 2013; Skutschas, 2013; Vasilyan et al., 2013), we limit our comparisons to species of Mesozoic salamanders (mostly Juro-Cretaceous species from China) known from complete or nearly complete skeletons and to the extant cryptobranchids *Andrias* and *Cryptobranchus*. Our phylogenetic analysis utilizes a broader range of extant salamander species from all living families and a modest selection of Mesozoic species represented by phylogenetically informative fossils, the latter mostly known by articulated skeletons.

6. Discussion

6.1. Chunerpeton compared with other Mesozoic taxa

With the possible exception of two paracontemporaneous species discussed in the latter part of this section, *Chunerpeton tianyiense* can be distinguished from all adequately known Mesozoic salamander species. It differs from the stem salamanders *Karaurus* and *Kokartus* (Jurassic, Central Asian) in lacking heavily-sculptured skull bones (Skutschas and Martin, 2011). Compared to crown salamanders, *Chunerpeton* differs from the Chinese Juro-Cretaceous species *Laccotriton subsolanus*, *Liaoxitriton daohugouensis*, *Liaoxitriton zhongjiani*, *Linglongtriton daxishanensis*, *Nuominerpeton aquilonare*, *Pangerpeton sinense*, and *Sinerpeton fengshanense* and the Spanish Cretaceous species *Valdotriton gracilis* in having: (1) pterygoid with a long, slender, and curved anteromedial process versus a shorter anteromedial process in all the listed taxa and (2) unossified tarsals and carpals versus ossified in most of the listed taxa, except *Pangerpeton* and *Valdotriton* (Evans and Milner, 1996; Dong and Wang, 1998; Gao and Shubin, 2001; Wang, 2004; Wang and Evans, 2006; Jia and Gao, 2016b, 2019). *Chunerpeton* further differs from *Pangerpeton*, as follows: (1) posteriorly elongate and narrow vomer versus triangular vomer with posterior extension in *Pangerpeton* and (2) 15 presacral vertebrae versus 14 presacral vertebrae in *Pangerpeton*. *Chunerpeton* further differs from *Valdotriton*, as follows: (1) premaxilla bearing a short pars praenasalis versus long pars dorsalis in *Valdotriton*; (2) unfused prootic, exoccipital, and opisthotic versus fused prootic, exoccipital, and opisthotic in *Valdotriton*; (3) unicapitate ribs versus bicapitate ribs in *Valdotriton*; and (4) single row of vomerine teeth versus two or three rows in *Valdotriton*. *Chunerpeton* can be further distinguished from *Regalerpeton weichangense* (Early Cretaceous, China), as follows: (1) long and narrow vomer with posterolaterally oriented vomerine tooth row versus roughly pentagonal vomer with transversely oriented vomerine tooth row in *Regalerpeton*; (2) separate opisthotic and exoccipital versus fused opisthotic and exoccipital in *Regalerpeton*; and (3) arrow-shaped basibranchial II versus triradiate in *Regalerpeton* (Rong, 2018). *Chunerpeton* differs from *Jeholotriton paradoxus* in having monostichous vomerine teeth versus multiple vomerine tooth rows in *Jeholotriton* (Wang and Rose, 2005). Finally, *Chunerpeton* differs from *Iridotriton hechti* (Late Jurassic, USA), as follows: (1) internal carotid foramina penetrating the parasphenoid versus internal carotid foramina absent from parasphenoid in *Iridotriton*; and (2) unfused prootic, exoccipital, and opisthotic versus three elements forming a single unit in *Iridotriton* (Evans et al., 2005).

More detailed comparisons are warranted between *Chunerpeton tianyiense* and two other neotenic and Chinese Jurassic species — *Beiyanerpeton jianpingense* and *Qinglongtriton gangouensis* for two reasons. First, Sullivan et al. (2014) and Wang et al. (2015) questioned whether fossils of *Chunerpeton* and *Beiyanerpeton* might belong to the same taxon, with *Chunerpeton* being the senior synonym. Although not previously expressed in print, similar questions also could be raised regarding the distinctiveness of *Chunerpeton* and *Qinglongtriton*. Second, in addition to being neotenic, all three taxa resemble each other in having (1) similarly shaped pterygoids, vomers, and parasphenoid; (2) the same suite of ossified hyobranchium elements; (3) palatine present in adults; (4) pterygoid bearing teeth; (5) and 15 presacral vertebrae (Gao and Shubin, 2012; Jia and Gao, 2016a). On the other hand, *Chunerpeton* appears to differ from the other two taxa, as follows: (1) unicapitate ribs versus probable bicapitate ribs in *Beiyanerpeton* and *Qinglongtriton* (Gao and Shubin, 2012; Jia and Gao, 2016a) and (2) arrow shaped basibranchial II versus arrow-shaped (juveniles) or anchor-shaped with two additional posterior spikes (adults) in *Qinglongtriton* (Jia and Gao, 2016a) and trident-shaped in *Beiyanerpeton* (Gao and Shubin, 2012). The above-listed two potential differences should be treated with caution. *Beiyanerpeton* and *Qinglongtriton* were reported to have weakly bicapitate ribs. It is important to mention that the proximal ends of some unicapitate ribs are grooved and, when their cartilaginous heads are lost, those ribs may erroneously appear weakly bicapitate. Apparent differences among the species in shapes of the basibranchial II may be at least partially ontogenetic. Although beyond the scope of our current paper, it is evident that more detailed comparisons are needed to resolve the taxonomic distinctiveness of the three species. For the purposes of our study, we accept *C. tianyiense*, *B. jianpingense*, and *Q. gangouensis* as distinct species.

6.2. Chunerpeton compared with living cryptobranchids

Osteological comparisons of *Andrias* (limited to *A. davidianus* and *A. japonicus*) and *Cryptobranchus alleganiensis* indicate that they share four synapomorphies: angular present, and no septomaxilla, lacrimal, or basibranchial II (Rose, 2003). Our observations on *Chunerpeton tianyiense* find that it shares two of those characters (angular present and septomaxilla absent) with living cryptobranchids, but *Chunerpeton* differs in having an ossified lacrimal and a basibranchial II.

During the course of our study, we noted numerous additional differences between *Chunerpeton* and extant cryptobranchids. When viewed in ventral or dorsal aspect, the snout of *Chunerpeton* is narrower than the maximum width of its head (as measured across the skull-mandible joints), whereas in extant cryptobranchids the snout is nearly as wide as the maximum width of the head (Fig. 4A, D, G). *Chunerpeton* further differs from extant cryptobranchids in an extensive suite of features related to the presence/absence, configurations, positions, and articulation of certain bones and hyobranchial bones, as follows: (1) pars praenasalis of premaxilla located in the middle of the bone (Fig. 4A) versus shifted towards the

medial end of the bone in cryptobranchids (Fig. 4D, G); (2) large, triangular nasals separated along the skull midline by an anterodorsal fenestra in *Chunerpeton* (Fig. 4A) versus narrow and elongate not separated by an anterodorsal fenestra and, instead, articulating with each other along the skull midline in cryptobranchids (Fig. 4D, G); (3) wide frontal not contacting the maxilla in *Chunerpeton* (Fig. 4A) versus narrow, elongate, and anteriorly curved frontal articulating with the pars facialis of the maxilla in cryptobranchids (Fig. 4D, G); (4) triangular prefrontal not contacting the parietal in *Chunerpeton* (Fig. 4A) versus long, narrow, and curved prefrontal articulating with the anterolateral process of parietal in cryptobranchids (Fig. 4D, G); (5) pterygoid bearing a long, slender, curved, and free anteromedial process and bearing a small, pointed, and free medial process in *Chunerpeton* (Fig. 4A) versus pterygoid bearing a shorter anteromedial process and bearing an enlarged medial process articulating with the orbitosphenoid in cryptobranchids (Fig. 4D, G); (6) broad and posteriorly elongate anterodorsal fenestra bordered by the premaxillae, nasals, and frontals in *Chunerpeton* (Fig. 4A) versus small anterodorsal fenestra located far anteriorly and bordered by the premaxillae and nasals in cryptobranchids (Fig. 4D, G); (7) lacrimal present in *Chunerpeton* (Fig. 4A) versus absent in cryptobranchids (Fig. 4D, G); (8) oval vomers, broadly separated across the skull midline, and with their long axis paralleling the premaxillae and maxillae, but not contacting those upper jaw bones in *Chunerpeton* (Fig. 4B) versus larger and triangular vomers articulating medially with each other and anteriorly with the premaxillae and maxillae in cryptobranchids (Fig. 4E, H); (9) large anteromedial fenestra forming by premaxillae, vomers, and parasphenoid in *Chunerpeton* (Fig. 4B) versus reduced anteromedial fenestra entirely enclosed by anterior portions of vomers in cryptobranchids (Fig. 4E, H); (10) single vomerine tooth row present and extending parallel to premaxillary and maxillary tooth rows in all taxa, but located in middle of vomer in *Chunerpeton* (Fig. 4B) versus located along anterolateral edge of vomer in cryptobranchids (Fig. 4E, H); (11) a small and free palatine present in *Chunerpeton* versus absent in extant cryptobranchids (Fig. 4E, H); (12) longer parasphenoid occupying posterior four-fifths of head length in *Chunerpeton* (Fig. 4B) versus shorter parasphenoid occupying posterior two-thirds of head length in cryptobranchids (Fig. 4E, H); (13) overlapping joint between premaxilla and maxilla in *Chunerpeton* (Fig. 4A) versus abutting joint between premaxilla and maxilla in

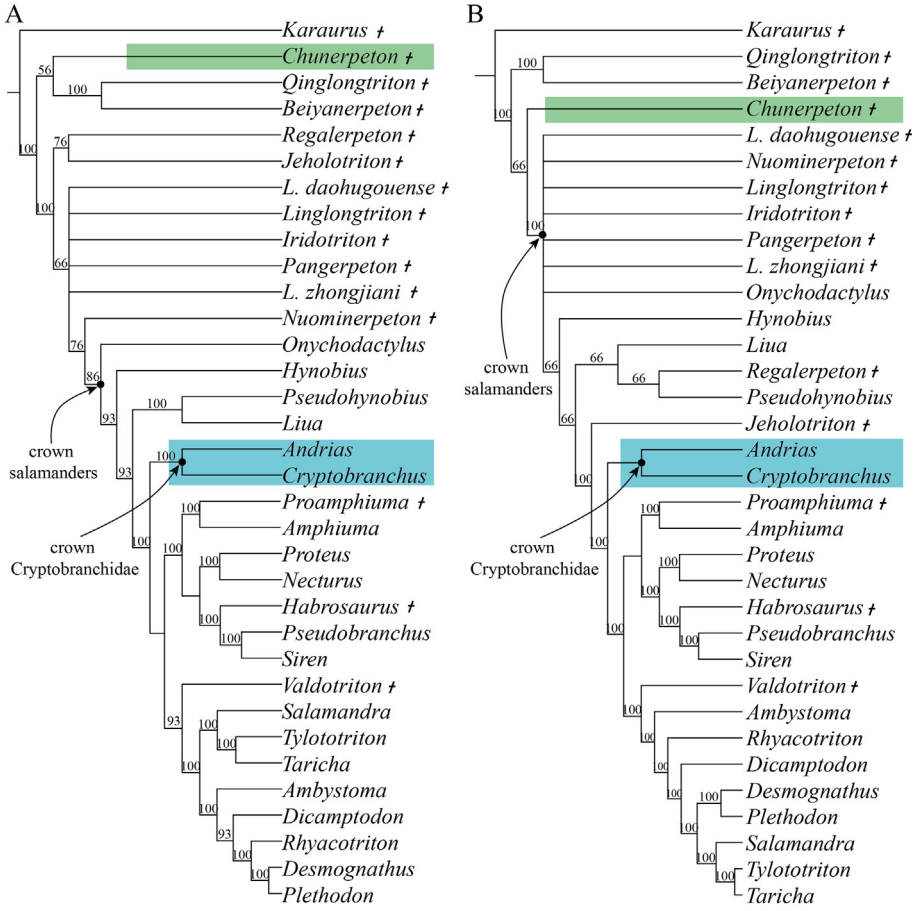

Fig. 5. Majority consensus trees showing positions of *Chunerpeton tianyiense* (in green) and crown Cryptobranchidae (in blue). (A) First analysis, generated using modified codings for *Chunerpeton*. (B) Second analysis, generated using modified codings for *Iridotriton* and *Jeholotriton*. See text for details and tree statistics.

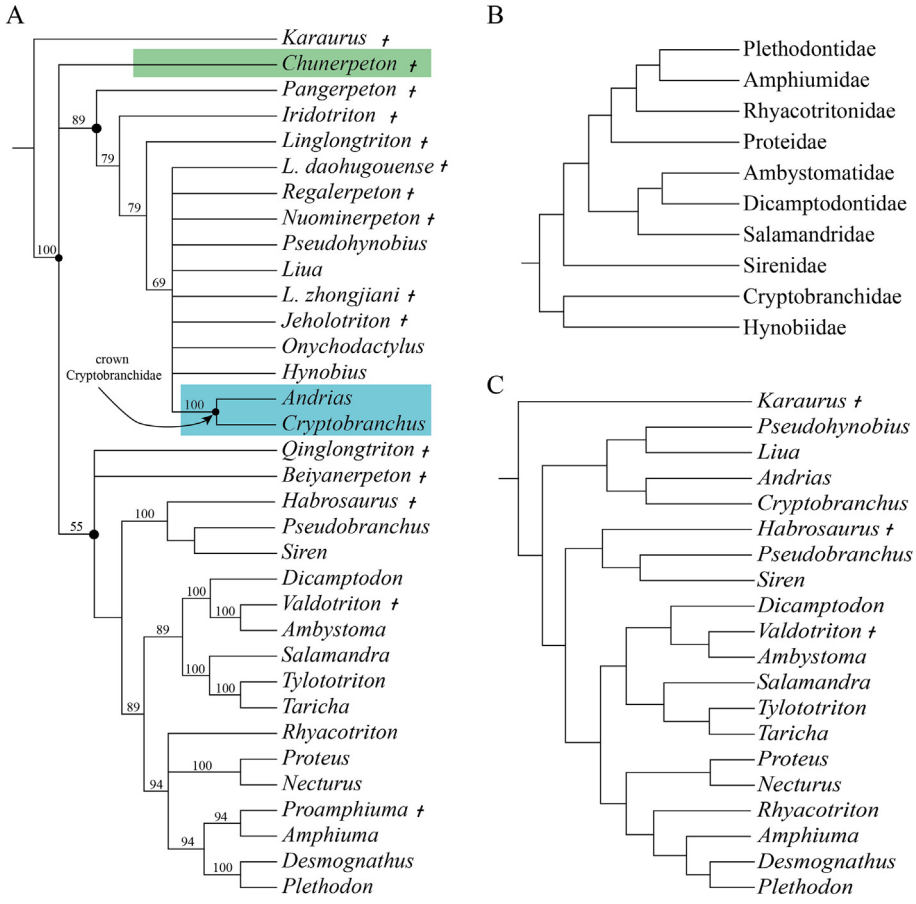

Fig. 6. (A) Majority rule consensus tree from third analysis, showing positions of *Chunerpeton tianyiense* (in green) and crown Cryptobranchidae (in blue). (B) Relationships among extant salamander families from Pyron and Wiens (2011), used as a molecular backbone to constrain the third analysis. (C) Agreement subtree from the fourth analysis, showing the largest subset of taxa (14 extant and three fossil) contained within the third analysis. See text for details and tree statistics.

cryptobranchids (Fig. 4D, G); (14) separate opisthotic and exoccipital in *Chunerpeton* (Fig. 4A) versus fused opisthotic and exoccipital in cryptobranchids (Fig. 4D, G); (15) ossified hyobranchium consisting of paired hypobranchials I and II and median basibranchial II in *Chunerpeton* (Fig. 4C) versus ossified hyobranchium consisting of paired hypobranchial II and ceratobranchial II in cryptobranchids (Fig. 4F, I). The presence of orbitosphenoids may be another difference. Ossified orbitosphenoids unequivocally are present in cryptobranchids (Fig. 4D, G), but have not reliably been identified in *Chunerpeton*. However, that difference may not stand if we are correct in our earlier suggestion that the holotype skull of *Chunerpeton* may preserve orbitosphenoids. Regardless of the distribution of the orbitosphenoid, the extensive suite of characters listed here clearly distinguishes *Chunerpeton* from extant cryptobranchids and raises further questions about whether *Chunerpeton* is related to Cryptobranchidae.

6.3. Phylogenetic relationships of *Chunerpeton*

We tested the phylogenetic position of *Chunerpeton* by running five sets of analyses using modified versions of the data matrix provided by Jia and Gao (2019), which consists of 120 characters (see Appendix A, Section 1) and 34 taxa. We ran our analyses in TNT version 1.5 (Goloboff and Catalano, 2016), using a traditional search of 100 000 replicates, 30 trees per replication, tree bisection-reconnection. We designated the stem salamander *Karaurus* as the outgroup and set all characters as unordered and equally weighted. Consistent with earlier analyses by Gao and Shubin (2012) and Jia and Gao (2019), we excluded eleven inapplicable characters (11, 18, 28, 47, 50, 72, 73, 92, 93, 103, and 109).

For our first analysis, we modified fourteen codings (Appendix A, Section 3) for *Chunerpeton* in the matrix of Jia and Gao (2019), based on the new fossils we examined. The result of this analysis produced 30 most parsimonious trees (tree length = 314; consistency index = 0.449; retention index = 0.718). The 50% majority consensus tree (Fig. 5A) recovers *Chunerpeton* as the sister to two contemporary Chinese taxa (*Beiyanerpeton* + *Qinglongtriton*). The existence of this clade of *Chunerpeton* + (*Beiyanerpeton* + *Qinglongtriton*) is supported by three synapomorphies: separate nasals without midline contact [character 8(1)]; well-developed anterolateral process of parietal sur-

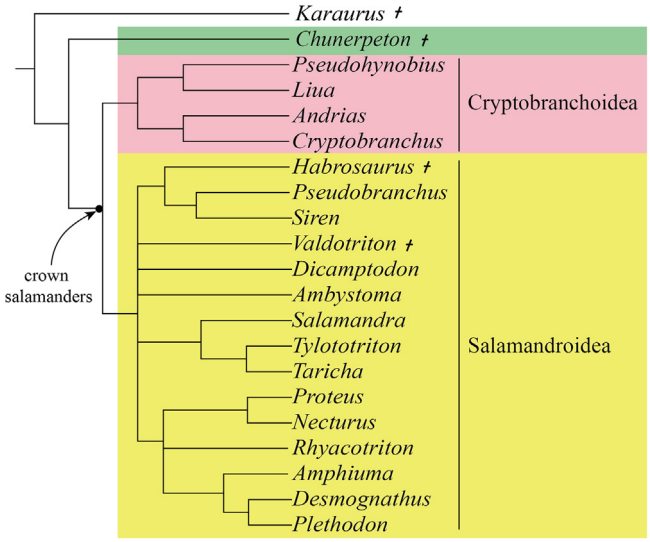

Fig. 7. Strict consensus tree from the fifth phylogenetic analysis, showing *Chunerpeton tianyiense* (in green) as a stem salamander and sister to crown salamanders, the latter consisting of Cryptobranchoidea (in pink) and Salamandroidea (in yellow). See text for details and tree statistics.

passing midlevel of the orbit [character 60(1)]; and anterodorsal fenestra bordered by the premaxilla, nasal and frontal [character 107(1)]. In contrast to previous proposals that *Chunerpeton* is closely related to, or a member of, Cryptobranchidae, our analysis places the clade of *Chunerpeton* + (*Beiyanerpeton* + *Qinglongtriton*) near the base of the tree, as the secondmost basal clade and removed from cryptobranchids. Other Mesozoic salamanders from China and *Iridotriton* fall out between the clade of *Chunerpeton* + (*Beiyanerpeton* + *Qinglongtriton*) and crown salamanders. Placement of *Chunerpeton* well outside of Cryptobranchidae and near the base of the tree is a consistent pattern in all our analyses that include *Chunerpeton*.

For our second analysis, we re-coded 23 characters for *Jeholotriton* and 33 characters for *Iridotriton* (Appendix A, Section 3), based on details in relevant publications (Evans et al., 2005; Wang and Rose, 2005; Carroll and Zheng, 2012), whereas both taxa were excluded in preceding study (Jia and Gao, 2019). Our second analysis produced 51 most parsimonious trees (tree length = 319; consistency index = 0.429; retention index = 0.708). The 50% majority consensus tree (Fig. 5B) retains the sister pair of *Beiyanerpeton* + *Qinglongtriton* in the same basal position, but shifts *Chunerpeton* one node crownward to become the sister to the remaining Mesozoic (except *Karaurus*) and all recent salamanders. Once again, *Chunerpeton* is far removed from crown Cryptobranchidae. As for the two re-coded taxa, *Iridotriton* remains in an unresolved polytomy with many Chinese Juro-Cretaceous taxa, whereas *Jeholotriton* shifts crownward to become the sister to a clade containing all non-hynobiid crown salamanders.

Because the family-level relations of living salamanders recovered in our first two analyses are inconsistent with molecular results (cf. Fig. 5A, B versus Fig. 6B), we performed a third analysis in which relationships of recent families were constrained by the molecular tree (Pyron and Wiens, 2011, Fig. 6B) and all fossil taxa are set as 'floaters'. That analysis produced 1211 most parsimonious trees and tree length equals to 344. The 50% majority consensus tree (Fig. 6A) recovers a trichotomy consisting of three groupings: *Chunerpeton* alone; a second clade consisting of *Beiyanerpeton*, *Qinglongtriton*, and salamandroids; and a third clade consisting of *Iridotriton*, the remaining Chinese Juro-Cretaceous salamanders, crown Cryptobranchidae, and a paraphyletic Hynobiidae. There are two differences among families compared to the molecular backbone (Fig. 6B). One is that hynobiids (*Onychodactylus*, *Hynobius*, *Pseudobranchus*, and *Liua*) fail to form a clade and the other is a trichotomy occurring between Proteidae (*Necturus* and *Proteus*), Rhyacotritonidae (*Rhyacotriton*) and Plethodontidae (*Desmognathus* and *Plethodon*) + Amphiumidae (*Amphiuma* and *Proamphiuma*). These differences may result from excessive parsimonious trees caused by problematic taxon or taxa.

In order to improve the resolution, we performed a fourth analysis by re-running our third analysis, but this time using the 'Agreement subtree' option, which aims to find the largest subset of taxa and to measure the similarity of these trees (Goloboff et al., 2008). The resultant agreement subtree (Fig. 6C) includes 17 of 19 recent taxa (the hynobiids *Hynobius* and *Onychodactylus* are excluded) and just three of the fossil taxa (*Karaurus*, *Habrosaurus*, and *Valdotriton*) from our previous analyses. The excluded fossil taxa consist of all the Juro-Cretaceous taxa from China (including *Chunerpeton*), the Jurassic *Iridotriton*, and the Late Cretaceous *Proamphiuma*. The agreement subtree (Fig. 6C) recovers an arrangement of families that exactly matches the molecular analysis presented in Fig. 6B, and *Habrosaurus* and *Valdotriton* are as the sister to crown sirenids and crown ambystomatids, respectively.

For our fifth and final analysis, we re-ran our analysis with the same 17 recent and four fossil taxa recovered in our agreement subtree and added *Chunerpeton* (i.e., essentially our third analysis, minus the problematic extant and fossil taxa). This analysis produced just two most parsimonious trees (tree length = 275; consistency index = 0.498; retention index = 0.779) that differ from one another only in the placement of *Valdotriton*, where one recovers *Valdotriton* as a stem salamandroid and the other as the sister to *Ambystoma*. The strict consensus tree (Fig. 7) recovers *Chunerpeton* as a stem-caudate and the sister of all crown salamanders, but there is no synapomorphy to support the clade of *Chunerpeton* + crown salamanders. Two synapomorphies support the "crown salamander" clade and exclude *Chunerpeton* from membership within that clade: anterior process of the maxilla elongated and extensively overlapped by the premaxilla [character 106(0)], and arrow-shaped basibranchial II [character 116(0)]. Cryptobranchidae is supported by nine autapomorphies:

anterodorsal fenestra present [character 6(0)]; nasals greatly reduced and narrower than frontals [character 9 (1)]; enlarged pterygoid with distinct anteromedial process suturing with the parasphenoid [character 16(1)]; contact between nasal and prefrontal absent [character 23(1)]; basibranchial II absent [character 35(1)]; articulation between pterygoid and parasphenoid present and along the anterior extension of the parasphenoid [character 44 (1)]; articulation between parietal and prefrontal present [character 61(1)]; contact between frontal and maxillary present [character 62(1)]; and anteroventral extension absent from ventral border of the orbitosphenoid [character 111(1)]. These nine characters of cryptobranchids are significantly different from *Chunerpeton* (detailed comparison is given above).

To determine whether the nine characters are constant for Cryptobranchidae, more detailed comparisons are warranted between cryptobranchids and other salamanders outside of this data matrix. A small anterodorsal fenestra formed by the premaxillae and nasals [character 6(0)] occurs in cryptobranchids (Fig. 4D, G), as well as in some salamandrids (Jia and Gao, 2019). A pair of small, elongated nasals narrower than frontals [character 9(1)] occurs in cryptobranchids (Fig. 4D, G), as well as in sirenids (Duellman and Trueb, 1994) and some hynobiids (e.g., *Salamandrella*; see Zhou et al., 2017: fig. 1e). However, there are two different cases: nasals articulating each other along the skull midline in cryptobranchids versus nasals separated along the skull midline in sirenids (Duellman and Trueb, 1994). An enlarged pterygoid with a distinct anteromedial process suturing with the parasphenoid [character 16(1)] occurs in cryptobranchids (Fig. 4E, H) and is a unique character for cryptobranchids (Gao and Shubin, 2012). No nasal-prefrontal contact [character 23(1)] occurs in cryptobranchids, as well as in some plethodontids (e.g., *Stereochilus marginatum*), some salamandrids (e.g., *Taricha granulosa*), and amphiumids (Duellman and Trueb, 1994). No basibranchial II [character 35(1)] occurs in cryptobranchids because the element disappears at early larval stages (Rose, 2003), as well as in salamandrids (e.g., *Notophthalmus viridescens*) where it is completely resorbed, and in amphiumids where it is never formed (Rose, 2003). A pterygoid-parasphenoid articulation along anterior extension of parasphenoid [character 44(1)] occurs in cryptobranchids (Fig. 4E, H), as well as in amphiumids, proteids, and *Pseudobranchus* (Gao and Shubin, 2012). A parietal-prefrontal articulation [character 61(1)] occurs in cryptobranchids (Fig. 4D, G), as well as in amphiumids and ambystomatids (Gao and Shubin, 2012). A frontal-maxilla contact [character 62(1)] occurs in cryptobranchids (Fig. 4D, G), as well as in some plethodontids (Duellman and Trueb, 1994). Absence of an anteroventral extension of the ventral border of the orbitosphenoid [character 111(1)] occurs in cryptobranchids, as well as in all known fossil taxa and some living hynobiids (Jia and Gao, 2019).

7. Conclusions

In this study, we restudied one of the earliest salamanders *Chunerpeton tianyiense* on the basis of recently collected fossil skeletons from the type locality. We provided currently the most detailed osteological description for the species, recognized a suite of new taxonomically and phylogenetically informative features (e.g., anterodorsal fenestra present and formed by premaxillae, nasals, and frontals; nasals without midline contact; nasal-prefrontal contact present; nasal wider than frontal; lacrimal present and contributing to external naris, but not to orbit; pterygoid triradiate with a slender dentate anteromedial process; single vomerine tooth row parallel to premaxillary and maxillary tooth rows; palatine present; prootic, exoccipital and opisthotic present as separate bones), and provided a revised diagnosis for the species.

We performed five phylogenetic analyses to reassess the phylogenetic position of *Chunerpeton* and, for the first time, we constrained a phylogenetic analysis that includes extinct salamanders by using a molecular backbone. Our results show that *Chunerpeton* is a stem salamander, consistently placed outside of both recent giant salamanders (Cryptobranchidae) and all crown salamanders. Our finding that the Jurassic *Chunerpeton* is not a cryptobranchid has two significant implications: (1) the origin of crown Cryptobranchidae and even Cryptobranchoidea might have occurred later than originally proposed by Gao and Shubin (2003), and (2) it is unsuitable to directly use *Chunerpeton* to calibrate a molecular clock in molecular studies of salamanders.

Acknowledgments

We are grateful to Wei Gao (IVPP) for photographing the specimen. We thank Pavel P. Skutschas, Susan E. Evans, and David Marjanović for their helpful comments and suggestions toward the improvement of earlier versions of the manuscript and Palaeoworld editors and anonymous reviewers for useful recommendations. We also thank James D. Gardner (Royal Tyrrell Museum of Palaeontology) for additional comments and helping with the English. This research was supported by the Strategic Priority Research Program (B) of the Chinese Academy of Sciences (Grant No. XDB18000000) and the National Natural Science Foundation of China (41688103), the Swiss National Science Foundation (Grant No. 181041), and the China Scholarship Council and Swiss Government Excellence Scholarship (2018–2019).

Supplementary data

Supplementary data to this article can be found online at https://doi.org/10.1016/j.palwor.2020.12.001.

References

Bossuyt, F., Brown, R.M., Hillis, D.M., Cannatella, D.C., Milinkovitch, M.C., 2006. Phylogeny and biogeography of a cosmopolitan frog radiation: Late Cretaceous diversification resulted in continent-scale endemism in the family Ranidae. Systematic Biology 55, 579–594.

Carroll, R.L., Holmes, R., 1980. The skull and jaw musculature as guides to the ancestry of salamanders. Zoological Journal of the Linnean Society 68, 1–40.

Carroll, R.L., Zheng, A., 2012. A neotenic salamander, *Jeholotriton paradoxus*, from the Daohugou Beds in Inner Mongolia. Zoological Journal of the Linnean Society 164 (3), 659–668.

Chen, M.Y., Mao, R.L., Liang, D., Kuro-o, M., Zeng, X.M., Zhang, P., 2015. A reinvestigation of phylogeny and divergence times of Hynobiidae (Amphibia, Caudata) based on 29 nuclear genes. Molecular Phylogenetics and Evolution 83, 1–6.

Dong, L.P., Huang, D.Y., Wang, Y., 2011. Two Jurassic salamanders with stomach contents from Inner Mongolia, China. Chinese Science Bulletin 57 (1), 72–76.

Dong, Z.M., Wang, Y., 1998. A new urodele (*Liaoxitriton zhongjiani* gen. et sp. nov.) from the Early Cretaceous of western Liaoning Province, China. Vertebrata PalAsiatica 36, 159–172 (in Chinese).

Duellman, W.E., Trueb, L. (Eds.), 1994. Biology of Amphibians. The Johns Hopkins University Press, Baltimore, 670 pp.

Evans, S.E., Milner, A.R., 1996. A metamorphosed salamander from the Early Cretaceous of Las Hoyas, Spain. Philosophical Transactions of the Royal Society B: Biological Sciences 351, 627–646.

Evans, S.E., Lally, C., Chure, D.C., Elder, A., Maisano, J.A., 2005. A Late Jurassic salamander (Amphibia: Caudata) from the Morrison Formation of North America. Zoological Journal of the Linnean Society 143, 599–616.

Francis, E.T.B. (Ed.), 1934. The Anatomy of the Salamander. Oxford University Press, Clarendon, 478 pp.

Gardner, J.D., DeMar Jr., D.G., 2013. Mesozoic and Palaeocene lissamphibian assemblages of North America: a comprehensive review. Palaeobiodiversity and Palaeoenvironments 93 (4), 459–515.

Gao, K.Q., Shubin, N.H., 2001. Late Jurassic salamanders from northern China. Nature 410, 574–577.

Gao, K.Q., Shubin, N.H., 2003. Earliest known crown-group salamanders. Nature 422, 424–428.

Gao, K.Q., Shubin, N.H., 2012. Late Jurassic salamandroid from western Liaoning, China. Proceedings of the National Academy of Sciences 109, 5767–5772.

Gao, K.Q., Chen, J.Y., Jia, J., 2013. Taxonomic diversity, stratigraphic range, and exceptional preservation of Juro-Cretaceous salamanders from northern China. Canadian Journal of Earth Sciences 50, 255–267.

Goloboff, P.A., Catalano, S.A., 2016. TNT version 1.5, including a full implementation of phylogenetic morphometrics. Cladistics 32, 221–238.

Goloboff, P.A., Farris, J.S., Nixon, K.C., 2008. TNT, a free program for phylogenetic analysis. Cladistics 24, 774–786.

Haeckel, E. (Ed.), 1866. Generelle Morphologie der Organismen. G. Reimer, Berlin, 626 pp. (in German).

Heiss, E., Grell, J., 2019. Same but different: aquatic prey capture in paedomorphic and metamorphic Alpine newts. Zoological Letters 5 (24), 1–12.

Huang, D.Y., 2015. Yanliao biota and Yanshan movement. Acta Palaeontologica Sinica 54, 501–546 (in Chinese).

International Commission on Zoological Nomenclature, 1999. International Code of Zoological Nomenclature, 4th Edition. Available at https://www.iczn.org/the-code/the-international-code-of-zoological-nomenclature/the-code-online/ (accessed on 29 June 2020).

Irisarri, I., Baurain, D., Brinkmann, H., Delsuc, F., Sire, J.-Y., Kupfer, A., Petersen, J., Jarek, M., Meyer, A., Vences, M., Philippe, H., 2017. Phylotranscriptomic consolidation of the jawed vertebrate timetree. Nature Ecology & Evolution 1 (9), 1370–1378.

Jia, J., Gao, K.Q., 2016a. A new basal salamandroid (Amphibia, Urodela) from the Late Jurassic of Qinglong, Hebei Province. China. PLOS ONE 11, e0153834, https://doi.org/10.1371/journal.pone. 0153834.

Jia, J., Gao, K.Q., 2016b. A new hynobiid-like salamander (Amphibia, Urodela) from Inner Mongolia, China, provides a rare case study of developmental features in an Early Cretaceous fossil urodele. PeerJ 4, e2499, https://doi.org/10.7717/peerj.2499.

Jia, J., Gao, K.Q., 2019. A new stem hynobiid salamander (Urodela, Cryptobranchoidea) from the Upper Jurassic (Oxfordian) of Liaoning Province, China. Journal of Vertebrate Paleontology 39 (2), e1588285, https://doi.org/10.1080/02724634.2019.1588285.

Linnaeus, C. (Ed.), 1758. Systema Naturae per regna tria naturae. Secundum classes, ordines, genera, species, cum characteribus, differentiis, synonymis, locis 1. Laurentius Salvius, Stockholm, 533 pp. (in Latin).

Liu, Y.Q., Liu, Y.X., Ji, S.A., Yang, Z.Q., 2006. U-Pb zircon age for the Daohugou Biota at Ningcheng of Inner Mongolia and comments on related issues. Chinese Science Bulletin 51, 2273–2282 (in Chinese, with English abstract).

Pyron, R.A., Wiens, J.J., 2011. A large-scale phylogeny of Amphibia including over 2800 species, and a revised classification of extant frogs, salamanders, and caecilians. Molecular Phylogenetics Evolution 61, 543–583.

Rong, Y.F., 2018. Restudy of *Regalerpeton weichangensis* (Amphibia: Urodela) from the Lower Cretaceous of Hebei, China. Vertebrata PalAsiatica 56, 121–136.

Rose, C.S., 2003. The developmental morphology of salamander skulls. In: Heatwole, H., Carroll, R.L. (Eds.), Amphibian Biology. Surrey Beatty & Sons, Chipping Norton, pp. 1684–1781.

San Mauro, D., Vences, M., Alcobendas, M., Zardoya, R., Meyer, A., 2005. Initial diversification of living amphibians predated the breakup of Pangaea. American Naturalist 165, 590–599.

Scopoli, G.A. (Ed.), 1777. Introductio ad historiam naturalem sistens genera lapidum, plantarum et animalium: hactenus detecta, caracteribus essentialibus donata, in tribus divisa, subinde ad leges naturae. Apud Wolfgangum Gerle, Prague, 547 pp. (in Latin).

Skutschas, P.P., 2013. Mesozoic salamanders and albanerpetontids of Middle Asia, Kazakhstan, and Siberia. Palaeobiodiversity and Palaeoenvironments 93 (4), 441–457.

Skutschas, P., Martin, T., 2011. Cranial anatomy of the stem salamander *Kokartus honorarius* (Amphibia: Caudata) from the Middle Jurassic of Kyrgyzstan. Zoological Journal of the Linnean Society 161, 816–838.

Sullivan, C., Wang, Y., Hone, W.E.D., Wang, Y.Q., Xu, X., Zhang, F.C., 2014. The vertebrates of the Jurassic Daohugou Biota of northeastern China. Journal of Vertebrate Paleontology 34 (2), 243–280.

Turvey, S.T., Marr, M.M., Barnes, I., Brace, S., Tapley, B., Murphy, R.W., Zhao, E., Cunningham, A.A., 2019. Historical museum collections clarify the evolutionary history of cryptic species radiation in the world's largest amphibians. Ecology and Evolution 9, 10070–10084.

Vasilyan, D., Böhme, M., Chkhikvadze, V.M., Semenov, Y.A., Joyce, W.G., 2013. A new giant salamander (Urodela, Pancryptobrancha) from the Miocene of Eastern Europe (Grytsiv, Ukraine). Journal of Vertebrate Paleontology 33, 301–318.

Wang, Y., 2004. A new Mesozoic caudate (*Liaoxitriton daohugouensis* sp. nov.) from Inner Mongolia, China. Chinese Science Bulletin 49, 858–860.

Wang, Y., Evans, S.E., 2006. A new short-bodied salamander from the Early Cretaceous of Liaoning, China. Acta Palaeontologica Polonica 51 (1), 127–130.

Wang, Y., Rose, C.S., 2005. *Jeholotriton paradoxus* (Amphibia: Caudata) from the Lower Cretaceous of southeastern Inner Mongolia, China. Journal of Vertebrate Paleontology 25, 523–532.

Wang, Y., Dong, L.P., Evans, S.E., 2015. Polydactyly and other limb abnormalities in the Jurassic salamander Chunerpeton

from China. Palaeobiodiversity and Palaeoenvironments 96, 49–59.

Wiens, J.J., Bonett, R.M., Chippindale, P.T., 2005. Ontogeny discombobulates phylogeny: paedomorphosis and higher-level salamander relationships. Systematic Biology 54, 91–110.

Zhang, G.L., Wang, Y., Jones, M.E.H., Evans, S.E., 2009. A new Early Cretaceous salamander (*Regalerpeton weichangensis* gen. et sp. nov.) from the Huajiying Formation of northeastern China. Cretaceous Research 30 (3), 551–558.

Zhou, Z.P., Fortuny, J., Marce-Nogue, J., Skutschas, P.P., 2017. Cranial biomechanics in basal urodeles: the Siberian salamander (*Salamandrella keyserlingii*) and its evolutionary and developmental implications. Scientific Reports 7, Article number 10174, doi: 10.1038/s41598-017-10553-1.